Crane load position control using Lyapunov-based pendulum damping and nonlinear MPC position control

Geir Ole Tysse and Olav Egeland

***Abstract*— A crane control system is presented where the crane load can track a position trajectory with ultimately bounded pendulum motions of the load. This is done with an inner loop using a Lyapunov-based damping controller which is designed to damp out the pendulum motions of the load, and an outer loop where a nonlinear MPC (model predictive controller) controls the position of the load. The Lyapunov-based damping controller is designed to be exponentially stable, which means that the pendulum motion will be ultimately bounded in the presence of a bounded perturbation. Then this is achieved by constraining the control action of the nonlinear MPC so that the perturbations to the Lyapunov-based damping controller are sufficiently bounded. The suspension point of the load, which is the tip of the crane, can then be controlled to track a time-varying desired trajectory in the plane with ultimately bounded pendulum motions. The control system is validated in simulations in a simulation study.**

I. INTRODUCTION

Cranes are important in marine operations, where high precision in hoisting operations is required. Significant payload oscillations may result from the motion of the crane and the crane base, and this can cause safety risks and suspension or delay of the operations. Automatic control of cranes and crane loads has the potential of reducing risk and execution time in marine operation. Control systems for crane has therefore been widely studied in the research community, and both open loop and closed loop control system strategies have been developed. Early work on crane control is found in [19] where optimal linear control is used in combination with a state observer. Extensive reviews are found in [1] and [17]. Sensor systems for the measurement of load motion as discussed in [18] is an important research topic for cranes. In this paper the focus will be on feedback control, and the sensor problem will not be further discussed.

Open loop control in the form of input shaping has been extensively studied for cranes [3], where the objective is to generate trajectories that will not excite pendulum motion. This was done by using the concept of flatness in [13], where smooth trajectories were generated for feedback control were generated, and where flatness lead to a simple model structure that could be controlled with pole placement. Moreover, acceleration inputs from the controller were converted to velocity inputs so that the velocity loops of the actuators could be used,. This was further developed in [18].

Nonlinear energy-based controllers of cart position and payload swing were proposed in [7] for a 2 DOF crane using LaSalle's invariance principle. In [4] the energy level was controlled for a 2-DOF overhead crane system. In [30] a nonlinear controller for payload position and oscillation in a 2-DOF gantry crane system was designed using a singular perturbation design. A nonlinear controller for a 4-DOF overhead crane and payload system is presented in [23]. In [29] the authors proposed a Lyapunov-based nonlinear controller with constrained trolley stroke and pendulum length, for a 4-DOF cart and payload system. In [5], [26] and [27] the authors proposed Lyapunov-based nonlinear controllers using feedback linearization, for positioning and swing suppression of the payload for a 3-DOF overhead crane. In [6] the payload was modelled as a bifilar pendulum which oscillated about the vertical axis, and a damping controller was designed based on LaSalle's invariance principle.

In [28] and [24] the authors applied MPC for controlling gantry cranes and overhead cranes with a trolley moving in one DOF. Another MPC-based scheme, which is referred as a particle swarm optimizer, was presented in [22] for a constrained control of underactuated payload. In [12] MPC was used in the vertical plane in combination with feedforward control for a crane with Maryland rigging to suppress the pendulum motion. In [2] a MPC was used for a mobile harbour crane to control the combined luffing and slewing motion, where real time solution of the MPC problem was achieved by linearizing the model about the desired trajectory. This work was further developed in [16] where flatness was used to simplify the dynamics, and by including the linearized feedforward part and a stabilizing feedback part.

In this paper we propose a Lyapunov-based controller for damping the oscillations of the crane payload in an inner loop, while the position of the crane tip is controlled in an outer loop using a nonlinear MPC. The Lyapunov-based controller is proved to be exponentially stable, and therefore ultimately bounded in the presence of a bounded perturbation. The bounded perturbations are determined by a nonlinear MPC for controlling the crane tip position. The crane tip can then be controlled to track a time-varying desired trajectory in the plane with ultimately bounded pendulum motions. The advantage of the method is that a robust and simple damping controller is used, and the resulting MPC problem is formulated without imposing state constraints so that it can be computed in real time. Moreover, the constraints of the MPC problem is on the perturbations to the damping controller, which further simplifies the MPC, and it can even be used for joy-stick input to commanded motion. In this paper a constant rope length is used, and the

[1]The authors are with the Department of Mechanical and Industrial Engineering, Norwegian University of Science and Technology (NTNU), N-7491 Trondheim, Norway. {geir.o.tysse,olav.egeland}@ntnu.no

crane tip moves in the horizontal plane.

The rest of this work is organized as follows. In Section II we present the spherical pendulum model. The Lyapunov-based damping controller is presented in Section III. In Section IV we present the nonlinear MPC. Some implementation aspects are discussed i Section V. Finally, the simulation results are presented in Section VI and the conclusions in Section VII.

II. Modeling

A. Kinematics

The inertial frame n is defined with the z axis pointing vertically downwards. The crane load is attached to a suspension point in the xy plane of n with position $\boldsymbol{r}_0^n = [x_0, y_0, 0]^{\mathrm{T}}$ in the coordinates of frame n. The crane load is modelled as a point mass m attached to the suspension point with a massless wire of length L. Frame b is fixed in the point mass of the load, and the motion of the load is modelled as a rotation of frame b about the suspension point with rotation matrix from n to b given by

$$\boldsymbol{R}_b^n = \boldsymbol{R}_x(\phi_x)\boldsymbol{R}_y(\phi_y) = \begin{bmatrix} c_y & 0 & s_y \\ s_x s_y & c_x & -s_x c_y \\ -c_x s_y & s_x & c_x c_y \end{bmatrix} \tag{1}$$

where $s_\alpha = \sin\alpha$, $c_\alpha = \cos\alpha$, $\boldsymbol{R}_x(\phi_x)$ is the rotation matrix for a rotation ϕ_x about the x axis, and $\boldsymbol{R}_y(\phi_y)$ describes the rotation ϕ_y about the current y axis. This is illustrated in Fig. 1. The position of the mass m in the coordinates of n is then $\boldsymbol{r}^n = \boldsymbol{r}_0^n + \boldsymbol{R}_b^n \boldsymbol{r}_r^b$, where $\boldsymbol{r}_r^b = [0, 0, L]^{\mathrm{T}}$ is the position of the point mass relative to the attachment point. It follows that the velocity of the point mass is

$$\boldsymbol{v}^n = \begin{bmatrix} \dot{x}_0 + Lc_y\dot{\phi}_y \\ \dot{y}_0 - Lc_xc_y\dot{\phi}_x + Ls_xs_y\dot{\phi}_y \\ -Ls_xc_y\dot{\phi}_x - Lc_xs_y\dot{\phi}_y \end{bmatrix}$$

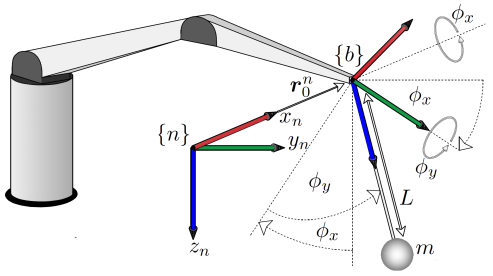

Fig. 1: Spherical pendulum and suspension point system with payload mass m and length of pendulum L

B. Equations of motion

The equations of motion for the load are found from Lagrange's equations of motion as in [1]. The kinetic energy of the pendulum is

$$K = \frac{1}{2}mL^2\left(\dot{\phi}_x^2 c_y^2 + \dot{\phi}_y^2\right) + \frac{1}{2}m\left(\dot{x}_0^2 + \dot{y}_0^2\right) + mL\dot{x}_0\dot{\phi}_y c_y - mL\dot{y}_0\left(\dot{\phi}_x c_x c_y - \dot{\phi}_y s_x s_y\right) \tag{2}$$

and the potential energy is

$$U = mgL(1 - c_x c_y) \tag{3}$$

The equations of motion can then be found from Lagrange's equation of motion, which gives the dynamic model

$$\ddot{\phi}_x c_y + \omega_0^2 s_x = 2\dot{\phi}_x\dot{\phi}_y s_y + \ddot{y}_0 c_x/L \tag{4}$$

$$\ddot{\phi}_y + \omega_0^2 c_x s_y = -\dot{\phi}_x^2 s_y c_y - (\ddot{x}_0 c_y + \ddot{y}_0 s_x s_y)/L \tag{5}$$

where $\omega_0^2 = g/L$ and g is the acceleration of gravity. The accelerations $\ddot{x}_0$ and $\ddot{y}_0$ of the suspension point are the control inputs of the system. This may pose some challenges in implementation as pointed out in [20]. This will be further discussed in the implementation part of the paper.

III. Controller design

A. Energy based damping controller

As a first step in the controller development for the pendulum a basic damping controller is proposed in this section. This controller solves the regulation problem of stabilizing the equilibrium point when the suspension point $\boldsymbol{r}_0^n$ is fixed. This damping controller will be the basis for the development of a more advanced tracking controller which will at the same time damp the pendulum motion and track the desired position of the point mass. This tracking controller will be presented in a later section. The basic damping controller is derived under the assumption that the acceleration $(\ddot{x}_0, \ddot{y}_0)$ of the suspension point in the horizontal plane can be used as control variables. The basic damping controller is given as the feedback control laws

$$\ddot{y}_0 = -2\zeta\omega_0 L\dot{\phi}_x \tag{6}$$

$$\ddot{x}_0 = 2\zeta\omega_0 L\dot{\phi}_y - \frac{\ddot{y}_0 s_x s_y}{c_y} \tag{7}$$

where ζ is a control parameter. Insertion of the control laws (6,7) into the equations of motion (4,5) gives

$$\ddot{\phi}_x c_y + 2\zeta\omega_0\dot{\phi}_x c_x + \omega_0^2 s_x = 2\dot{\phi}_x\dot{\phi}_y s_y \tag{8}$$

$$\ddot{\phi}_y + 2\zeta\omega_0\dot{\phi}_y c_y + \omega_0^2 c_x s_y = -\dot{\phi}_x^2 s_y c_y \tag{9}$$

It is noted that linearization about the equilibrium point $\phi_x = \phi_y = 0$ and $\dot{\phi}_x = \dot{\phi}_y = 0$ gives

$$\ddot{\phi}_x + 2\zeta\omega_0\dot{\phi}_x + \omega_0^2\phi_x = 0 \tag{10}$$

$$\ddot{\phi}_y + 2\zeta\omega_0\dot{\phi}_y + \omega_0^2\phi_y = 0 \tag{11}$$

It is seen that the linearized system is two harmonic oscillators with undamped natural frequency ω_0 and relative damping ζ.

The stability of the nonlinear closed loop dynamics (8,9) can be analyzed with the energy function

$$V_d = \frac{1}{2}mL^2\left(\dot{\phi}_x^2 c_y^2 + \dot{\phi}_y^2\right) + mgL(1 - c_x c_y) \tag{12}$$

which is the kinetic plus potential energy of the pendulum when the suspension point is stationary. The time derivative along the trajectories of equations of motion (4,5) is

$$\dot{V}_d = mL\dot{\phi}_x\ddot{y}_0 c_y c_x - mL\dot{\phi}_y\left(\ddot{x}_0 c_y + \ddot{y}_0 s_x s_y\right) \tag{13}$$

Insertion of the control laws (6,7) gives the time derivative of V_d along the trajectories of the closed loop dynamics (8,9) as

$$\dot{V}_d = -2\zeta\omega_0 mL^2\left(\dot{\phi}_x^2 c_x c_y + \dot{\phi}_y^2 c_y\right) \tag{14}$$

From LaSalle's theorem it follows that the equilibrium point $\phi_x = \phi_y = 0$ and $\dot{\phi}_x = \dot{\phi}_y = 0$ of the closed loop dynamics (8,9) is asymptotically stable. It is noted that this result is only valid for the regulation problem of stabilizing the pendulum about the equilibrium point.

B. Lyapunov-Based Tracking Controller

The second step in the controller development is to design an exponentially stable Lyapunov controller for the pendulum motion in ϕ_x and ϕ_y. The accelerations are considered as the control variables, and are written $\ddot{x}_0 = u_x$ and $\ddot{y}_0 = u_y$. Consider the feedback control laws

$$u_y = -\frac{Lc_y}{c_x}(k_d\dot{\phi}_x + k_p\phi_x) - \frac{2Ls_y}{c_x}\dot{\phi}_x\dot{\phi}_y + g\frac{s_x s_y^2}{c_x} \tag{15}$$

$$u_x = \frac{L}{c_y}(k_d\dot{\phi}_y + k_p\phi_y) - Ls_y\dot{\phi}_x^2 - \frac{u_y s_x s_y}{c_y} \tag{16}$$

which is a combination of PD control with feedback from the angle and the rate of the angle, and cancellation terms. The terms k_p and k_d are control gains. It is noted that the cancellation terms are higher-order terms, which will be small. Insertion of the control laws (15, 16) into the equation of motion (4, 5) gives the closed loop dynamics

$$\ddot{\phi}_x + k_d\dot{\phi}_x + k_p\phi_x + \omega_0^2 c_y s_x = 0 \tag{17}$$

$$\ddot{\phi}_y + k_d\dot{\phi}_y + k_p\phi_y + \omega_0^2 c_x s_y = 0 \tag{18}$$

where it is used that $c_y s_x = s_x/c_y - s_x s_y^2/c_y$.

C. Lyapunov function

Let the state vector be $\boldsymbol{x} = [\phi_x, \dot{\phi}_x, \phi_y, \dot{\phi}_y]^{\mathrm{T}}$. We will use the Lyapunov function

$$V(\boldsymbol{x}) = \frac{1}{2}\boldsymbol{x}^{\mathrm{T}}\boldsymbol{P}\boldsymbol{x} + mgL\left(1 - c_x c_y\right)$$

where $\boldsymbol{P}$ is a real symmetric positive definite matrix given by

$$\boldsymbol{P} = \begin{bmatrix} p_{11} & p_{13} & 0 & 0 \\ p_{13} & p_{22} & 0 & 0 \\ 0 & 0 & p_{11} & p_{13} \\ 0 & 0 & p_{13} & p_{22} \end{bmatrix} \tag{19}$$

where

$$p_{11} = (k_p + ck_d)p_{22}, \quad p_{13} = cp_{22}, \quad p_{22} = mL^2 \tag{20}$$

and c is a positive constant which satisfies $c < k_d$. It is noted that

$$p_{11} - p_{13}k_d - p_{22}k_p = 0 \tag{21}$$

The nonzero p_{13} gives cross terms in the Lyapunov function as introduced by [25]. From $p_{11} > 0$ and

$$\begin{vmatrix} p_{11} & p_{13} \\ p_{13} & p_{22} \end{vmatrix} = \left((k_p + ck_d) - c^2\right)p_{22}^2 > 0 \tag{22}$$

it can be concluded that the matrix $\boldsymbol{P}$ is positive definite [9], which implies that the eigenvalues of $\boldsymbol{P}$ are positive.

Consider the domain

$$D = \left\{\boldsymbol{x} \mid |\phi_x| < \frac{\pi}{2} - \delta \text{ and } |\phi_y| < \frac{\pi}{2} - \delta\right\} \tag{23}$$

where $0 < \delta < \pi/2$. Since $mgL\left(1 - c_x c_y\right) \geq 0$ in the domain D, it follows from (19) that

$$\frac{1}{2}\boldsymbol{x}^{\mathrm{T}}\boldsymbol{P}\boldsymbol{x} \leq V(\boldsymbol{x}) \quad \forall \boldsymbol{x} \in D \tag{24}$$

It follows that

$$\frac{1}{2}\lambda_{\min}(\boldsymbol{P})||\boldsymbol{x}||_2^2 \leq V(\boldsymbol{x}), \quad \forall \boldsymbol{x} \in D \tag{25}$$

where $\lambda_{\min}(\boldsymbol{P}) > 0$ is the smallest eigenvalue of $\boldsymbol{P}$. From $|\sin\alpha| \leq |\alpha|$ it follows that $\sin^2(\alpha/2) \leq \alpha^2/4$. In combination with $\cos\alpha = 1 - 2\sin^2(\alpha/2)$, this gives $\cos\alpha \geq 1 - \alpha^2/2$. Then it is straightforward to verify that

$$(1 - c_x c_y) \leq \frac{1}{2}\left(\phi_x^2 + \phi_y^2\right), \quad \forall\, \boldsymbol{x} \in D \tag{26}$$

From this, it follows that

$$V(\boldsymbol{x}) \leq \frac{1}{2}\boldsymbol{x}^{\mathrm{T}}\tilde{\boldsymbol{P}}\boldsymbol{x} \tag{27}$$

where $\tilde{\boldsymbol{P}} = \boldsymbol{P} + mgL\,\mathrm{diag}(1, 0, 1, 0)$. From (25) and (27), it is seen that the Lyapunov function is upper and lower bounded by

$$k_1||\boldsymbol{x}||_2^2 \leq V(\boldsymbol{x}) \leq k_2||\boldsymbol{x}||_2^2, \quad \forall \boldsymbol{x} \in D \tag{28}$$

where $k_1 = (1/2)\lambda_{\min}(\boldsymbol{P})$ and $k_2 = (1/2)\lambda_{\max}(\tilde{\boldsymbol{P}})$. It is concluded that the Lyapunov function $V(\boldsymbol{x})$ in (28) is positive definite and decrescent in the domain D. This is illustrated in Fig. 2 with gains $k_p = 0.1$ and $k_d = 2\sqrt{k_p}$.

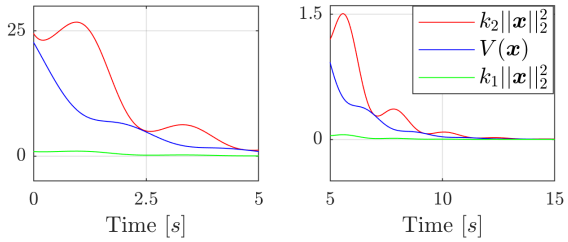

Fig. 2: The Lyapunov function $V(\boldsymbol{x})$ is lower bounded by $k_1||\boldsymbol{x}||_2^2$ and upper bounded by $k_2||\boldsymbol{x}||_2^2$ for $\boldsymbol{x} \in D$. Note that the right window is a continuation of the left window, but with different scale.

D. Derivative of Lyapunov function

The time derivative of $V(\boldsymbol{x})$ along the solutions of the closed loop dynamics (17, 18) is given by

$$\begin{aligned}\dot{V}(\boldsymbol{x}) = &\left(\dot{\phi}_x\phi_x + \dot{\phi}_y\phi_y\right)p_{11} \\ &- \left(p_{13}\phi_x + p_{22}\dot{\phi}_x\right)\left(k_d\dot{\phi}_x + k_p\phi_x + \omega_0^2 s_x c_y\right) \\ &- \left(p_{13}\phi_y + p_{22}\dot{\phi}_y\right)\left(k_d\dot{\phi}_y + k_p\phi_y + \omega_0^2 c_x s_y\right) \\ &+ mgL\dot{\phi}_y c_x s_y + mgL\dot{\phi}_x s_x c_y \\ = &\left(\dot{\phi}_x\phi_x + \dot{\phi}_y\phi_y\right)\left(p_{11} - p_{13}k_d - p_{22}k_p\right) \\ &- p_{13}k_p(\phi_x^2 + \phi_y^2) - p_{22}k_d(\dot{\phi}_x^2 + \dot{\phi}_y^2) \\ &- p_{13}\omega_0^2\left(\phi_x s_x c_y + \phi_y s_y c_x\right) \\ &+ \left(\dot{\phi}_x s_x c_y + \dot{\phi}_y c_x s_y\right)\left(mgL - p_{22}\omega_0^2\right) \end{aligned} \tag{29}$$

Then, from (20) and (21) it follows that

$$\begin{aligned}\dot{V}(\boldsymbol{x}) = &-p_{13}k_p(\phi_x^2 + \phi_y^2) - p_{22}k_d(\dot{\phi}_x^2 + \dot{\phi}_y^2) \\ &- p_{13}\omega_0^2\left(\phi_x s_x c_y + \phi_y s_y c_x\right)\end{aligned} \tag{30}$$

It is straightforward to verify that $\phi_x s_x c_y + \phi_y c_x s_y \geq 0$ in D. This gives

$$\dot{V}(\boldsymbol{x}) \leq -p_{13}k_p(\phi_x^2 + \phi_y^2) - p_{22}k_d(\dot{\phi}_x^2 + \dot{\phi}_y^2) \tag{31}$$

and it follows that

$$\dot{V}(\boldsymbol{x}) \leq -k_3||\boldsymbol{x}||_2^2 \tag{32}$$

where $k_3 = \min\{p_{13}k_p, p_{22}k_d\}$. This is illustrated in Fig. 3 for $k_p = 0.1$ and $k_d = 2\sqrt{k_p}$. Then, we can conclude that the closed loop dynamics (17,18) are exponentially stable in D.

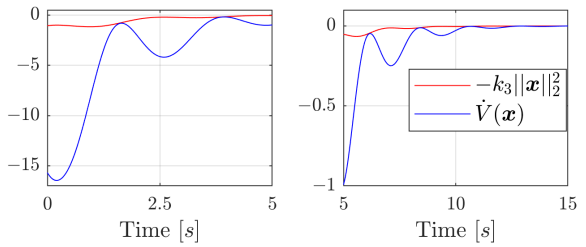

Fig. 3: The derivative of the Lyapunov function $\dot{V}(\boldsymbol{x})$ is upper bounded by $-k_3||\boldsymbol{x}||_2^2$ for all $\boldsymbol{x} \in D$. Note that the right window is a continuation of the left window, but with different scale.

E. Non-vanishing Perturbation

In practice it will not be possible to assign input values to the acceleration $(\ddot{x}_0, \ddot{y}_0)$ of the suspension point. To account for this, the acceleration of the suspension point is modelled as

$$\ddot{x}_0 = u_x + g_x \tag{33}$$

$$\ddot{y}_0 = u_y + g_y \tag{34}$$

where (u_x, u_y) are the controls assigned to the accelerations according to the control laws (15,16), and (g_x, g_y) are the deviations in acceleration from the assigned input values. The variables (g_x, g_y) are called non-vanishing perturbations as described in [11]. The closed loop dynamics will then be

$$\ddot{\phi}_x + k_d\dot{\phi}_x + k_p\phi_x + \omega_0^2 c_y s_x - \frac{c_x}{c_y L}g_y = 0 \tag{35}$$

$$\ddot{\phi}_y + k_d\dot{\phi}_y + k_p\phi_y + \omega_0^2 c_x s_y + \frac{c_y}{L}g_x + \frac{s_x s_y}{L}g_y = 0 \tag{36}$$

The time derivative of $V(\boldsymbol{x})$ along the trajectories of (35, 36) will then satisfy

$$\begin{aligned}\dot{V}(\boldsymbol{x}) &\leq -k_3||\boldsymbol{x}||_2^2 + \frac{c_x}{c_y L}(p_{13}\phi_x + p_{22}\dot{\phi}_x)g_y \\ &\quad - \frac{1}{L}(p_{13}\phi_y + p_{22}\dot{\phi}_y)(c_y g_x + s_x s_y g_y) \\ &\leq -k_3||\boldsymbol{x}||_2^2 + \alpha_x g_x + \alpha_y g_y\end{aligned} \tag{37}$$

where

$$\alpha_x = -\frac{c_y}{L}(p_{13}\phi_y + p_{22}\dot{\phi}_y) \tag{38}$$

$$\alpha_y = -\frac{s_x s_y}{L}(p_{13}\phi_y + p_{22}\dot{\phi}_y) + \frac{c_x}{c_y L}(p_{13}\phi_x + p_{22}\dot{\phi}_x) \tag{39}$$

It is assumed that the perturbations g_x and g_y in the commanded accelerations (33, 34) are uniformly bounded and satisfy

$$|g_x(t)| \leq \gamma \quad \text{and} \quad |g_y(t)| \leq \gamma, \quad \forall t \geq 0 \tag{40}$$

Then, the time derivative along the trajectories of (35,36) will satisfy

$$\dot{V}(\boldsymbol{x}) \leq -k_3||\boldsymbol{x}||_2^2 + \gamma\left(\alpha_x + \alpha_y\right) \tag{41}$$

where α_x and α_y satisfy

$$\alpha_x \leq \frac{c_y}{L}(p_{13}|\phi_y| + p_{22}|\dot{\phi}_y|) \leq \frac{1}{L}(p_{13}|\phi_y| + p_{22}|\dot{\phi}_y|) \tag{42}$$

and

$$\begin{aligned}\alpha_y \leq &\frac{|s_x s_y|}{L}(p_{13}|\phi_y| + p_{22}|\dot{\phi}_y|) + \frac{c_x}{Lc_y}(p_{13}|\phi_x| + p_{22}|\dot{\phi}_x|) \\ \leq &\frac{p_{13}|\phi_y| + p_{22}|\dot{\phi}_y|}{L} + \frac{p_{13}|\phi_x| + p_{22}|\dot{\phi}_x|}{c_1 L}\end{aligned} \tag{43}$$

where $c_1 = \cos(\pi/2 - \delta) \leq c_y, \forall \boldsymbol{x} \in D$, and where it is used that $|c_x| \leq 1$, $|c_y| \leq 1$ and $|s_x s_y| \leq 1$. It follows that

$$\begin{aligned}\alpha_x + \alpha_y &\leq \frac{p_{13}}{c_1 L}|\phi_x| + \frac{p_{22}}{c_1 L}|\dot{\phi}_x| + \frac{2p_{13}}{L}|\phi_y| + \frac{2p_{22}}{L}|\dot{\phi}_y| \\ &\leq k_4||\boldsymbol{x}||_2\end{aligned} \tag{44}$$

where

$$k_4 = \frac{1}{c_1 L}\sqrt{(4c_1^2 + 1)(p_{13}^2 + p_{22}^2)} \tag{45}$$

Then, with $0 < \theta < 1$, the time derivative of $V(\boldsymbol{x})$ along the trajectories of (35, 36) will satisfy

$$\begin{aligned}\dot{V}(\boldsymbol{x}) &\leq -k_3||\boldsymbol{x}||_2^2 + k_4\gamma||\boldsymbol{x}||_2 \\ &\leq -(1-\theta)\,k_3||\boldsymbol{x}||_2^2 - \theta k_3||\boldsymbol{x}||_2^2 + k_4\gamma||\boldsymbol{x}||_2 \\ &\leq -(1-\theta)\,k_3||\boldsymbol{x}||_2^2, \quad \forall\,||\boldsymbol{x}||_2 \geq \frac{\gamma k_4}{\theta k_3}\end{aligned} \tag{46}$$

This is illustrated in Fig. 4 with $\theta = 0.8$ and gains $k_p = 10$ and $k_d = 2\sqrt{k_p}$. The perturbations (g_x, g_y) applied to (35, 36) in this simulation, were high frequent rectangular pulse trains with amplitude/constraint $\gamma = 2$ ms^{-2}. In the upper windows of Fig. 4, it is seen that $||\boldsymbol{x}||_2 \geq \gamma k_4 / (\theta k_3)$ is valid in $t \leq T_1$. In the lower windows of Fig. 4, it is seen that $\dot{V}(\boldsymbol{x}) \leq -(1-\theta)\, k_3 ||\boldsymbol{x}||_2^2$ is valid in $t \leq T_1$. It is also seen that $\dot{V}(\boldsymbol{x}) \leq -k_3||\boldsymbol{x}||_2^2 + k_4\gamma||\boldsymbol{x}|_2$ for $\forall\, t$. The solution of

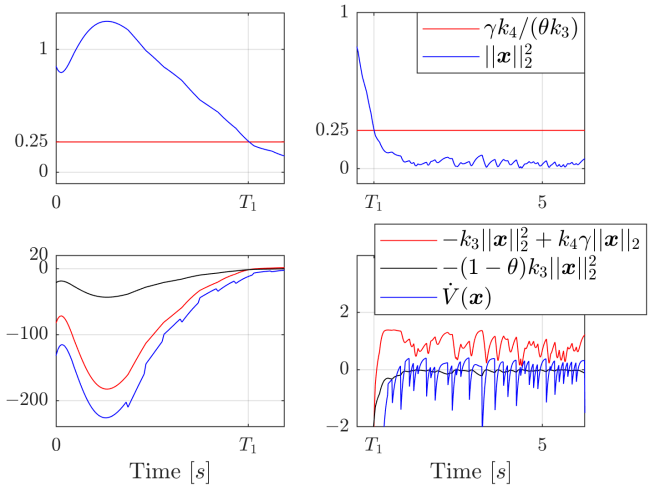

Fig. 4: Illustration of the ultimate boundedness of the norm of the state for a simple case study. Upper left and right: It is seen that $||\boldsymbol{x}||_2 \geq \gamma k_4 / (\theta k_3)$ is valid in $t \leq T_1$. Lower left and right: It is seen that $\dot{V}(\boldsymbol{x}) \leq -(1-\theta)\, k_3 ||\boldsymbol{x}||_2^2$ is valid in $t \leq T_1$ and $\dot{V}(\boldsymbol{x}) \leq -k_3||\boldsymbol{x}||_2^2 + k_4\gamma||\boldsymbol{x}|_2$ for $\forall\, t$. Note that the upper right and lower right windows are continuation of the upper left and lower left windows, but with different scales.

the perturbed system (35, 36) satisfies

$$||\boldsymbol{x}(t)||_2 \leq ke^{-\varphi t}||\boldsymbol{x}(0)||_2, \quad \forall\, t < T \tag{47}$$

and

$$||\boldsymbol{x}(t)||_2 \leq b, \quad \forall\, t \geq T \tag{48}$$

for some finite T, where

$$k = \sqrt{\frac{k_2}{k_1}}, \quad \varphi = \frac{(1-\theta)k_3}{2k_2}, \quad b = \frac{k_4}{k_3}\sqrt{\frac{k_2}{k_1}}\frac{\gamma}{\theta} \tag{49}$$

IV. Nonlinear MPC

The control laws (15, 16) are used to damp the pendulum motion of the load mass using the acceleration $(\ddot{x}_0, \ddot{y}_0)$ of the suspension point. In this section the functionality of the controller is extended so that also the position (x_0, y_0) of the suspension point can be controlled in the horizontal plane. The motivation for this is that if the position of the suspension point can be controlled, and the pendulum motion of the mass can be damped, then the position of the load mass can be controlled. Using the control laws (15, 16) in an inner loop, the position of the suspension point is controlled using the perturbations g_x and g_y of the accelerations in (33, 34) as control variables of the closed loop system (35, 36). The dynamics of the system is then

$$\ddot{x}_0 = g_x + \frac{L(k_d\dot{\phi}_y + k_p\phi_y) - Lc_y s_y \dot{\phi}_x^2 - u_y s_x s_y}{c_y} \tag{50}$$

$$\ddot{y}_0 = g_y - \frac{Lc_y(k_d\dot{\phi}_x + k_p\phi_x) + 2Ls_y\dot{\phi}_x\dot{\phi}_y - g s_x s_y^2}{c_x} \tag{51}$$

$$\ddot{\phi}_x = -k_d\dot{\phi}_x - k_p\phi_x - \omega_0^2 c_y s_x + \frac{c_x}{c_y L} g_y \tag{52}$$

$$\ddot{\phi}_y = -k_d\dot{\phi}_y - k_p\phi_y - \omega_0^2 c_x s_y - \frac{c_y}{L} g_x - \frac{s_x s_y}{L} g_y \tag{53}$$

We introduce a state vector

$$\boldsymbol{z} = \begin{bmatrix} x_0 & \dot{x}_0 & y_0 & \dot{y}_0 & \phi_x & \dot{\phi}_x & \phi_y & \dot{\phi}_y \end{bmatrix}^{\mathrm{T}} \tag{54}$$

and the non-vanishing perturbations g_x and g_y as the elements of the control vector

$$\boldsymbol{w} = \begin{bmatrix} g_x & g_y \end{bmatrix}^{\mathrm{T}} \tag{55}$$

The state space model is written

$$\dot{\boldsymbol{z}}(t) = \boldsymbol{f}(\boldsymbol{z}(t), \boldsymbol{w}(t)), \quad \boldsymbol{z}(0) = \boldsymbol{z}_0 \tag{56}$$

where the elements of $\boldsymbol{f}$ are found from (50–53). We consider the stabilization problem of the system in (56) subjected to input constraint

$$\boldsymbol{w}(t) \in \mathbb{U}, \ \forall t \geq 0 \tag{57}$$

where

$$\mathbb{U} := \{\boldsymbol{w} \mid |g_x| < \gamma \text{ and } |g_y| < \gamma\} \tag{58}$$

Based on the state $\boldsymbol{z}(t)$ sampled at time t, the NMPC predicts the future dynamic behaviour of the system (56) over a prediction horizon T_p and determines the control inputs $\boldsymbol{w}$ such that a predetermined open-loop performance objective functional is optimized. In order to incorporate a feedback mechanism, the control input $\boldsymbol{w}$ will be valid only until the next sample of $\boldsymbol{z}(t)$ becomes available, at which time a new control is calculated. In order to distinguish clearly between the real system (56) and the system model used to predict the future within the controller, we denote the internal variables in the controller by a bar (for example $\bar{\boldsymbol{z}}$, $\bar{\boldsymbol{w}}$). The required format for the NMPC controller is a discrete-time model [8], [10]. The discrete-time model of (56) used to predict the future, is

$$\bar{\boldsymbol{z}}_{k+1} = \boldsymbol{f}_k(\bar{\boldsymbol{z}}_k, \bar{\boldsymbol{w}}_k), \ \bar{\boldsymbol{z}}_0 = \boldsymbol{z}(t), \ k = 0, ..., M-1 \tag{59}$$

where the time step is $h = T_p/M$ with M prediction steps and prediction horizon T_p. To achieve a better accuracy of the discrete model [15], we use a repeated application of Euler's method sampled at a much higher rate $\Delta = h/P$, according to Algorithm 1. Based on this dynamic system form, we regard the following simplified NMPC optimization control problem in discrete time

$$\min_{\bar{\boldsymbol{w}}_k} J\left(\boldsymbol{z}(t), \bar{\boldsymbol{w}}(\cdot)\right) := \sum_{k=0}^{M-1} (\bar{\boldsymbol{z}}_k - \bar{\boldsymbol{z}}_r)^{\mathrm{T}} \boldsymbol{Q} (\bar{\boldsymbol{z}}_k - \bar{\boldsymbol{z}}_r) \tag{60}$$

Algorithm 1 $\bar{\boldsymbol{z}}_{k+1} = \boldsymbol{f}_k(\bar{\boldsymbol{z}}_k, \bar{\boldsymbol{w}}_k)$

$\Delta = h/P$
$\hat{\boldsymbol{z}}_0 = \bar{\boldsymbol{z}}_k$
for $i \in \{0, ..., P-1\}$ **do**
    $\hat{\boldsymbol{z}}_{i+1} = \hat{\boldsymbol{z}}_i + \Delta \boldsymbol{f}(\hat{\boldsymbol{z}}_i, \bar{\boldsymbol{w}}_k)$
end for
$\bar{\boldsymbol{z}}_{k+1} = \hat{\boldsymbol{z}}_P$

$$\begin{aligned} \text{subjected to} \quad \bar{\boldsymbol{z}}_0 &= \boldsymbol{z}(t) \\ \bar{\boldsymbol{z}}_{k+1} &= \boldsymbol{f}_k(\bar{\boldsymbol{z}}_k, \bar{\boldsymbol{w}}_k), \quad k = 0, ..., M-1 \\ \bar{\boldsymbol{z}}_r &= \boldsymbol{z}_r(t) \\ \bar{\boldsymbol{w}}_k &\in \mathbb{U}, \quad k = 0, ..., M-1 \end{aligned} \tag{61}$$

Here,

$$\boldsymbol{z}_r = \begin{bmatrix} x_r & \dot{x}_r & y_r & \dot{y}_r & 0 & 0 & 0 & 0 \end{bmatrix}^{\mathrm{T}} \tag{62}$$

is a pre-defined reference to the state $\boldsymbol{z}$. The positive semidefinite matrix

$$\boldsymbol{Q} = \mathrm{diag}(Q_{x_0}, Q_{\dot{x}_0}, Q_{y_0}, Q_{\dot{y}_0}, 0, 0, 0, 0) \tag{63}$$

defines the weights on the error between actual suspension point position and velocity $(x_0, \dot{x}_0, y_0, \dot{y}_0)$ and desired position and velocity $(x_r, \dot{x}_r, y_r, \dot{y}_r)$. The states $\{\bar{\boldsymbol{z}}_1, ..., \bar{\boldsymbol{z}}_M\}$ are the solutions of (59) driven by the control inputs $\bar{\boldsymbol{w}}(\cdot; \boldsymbol{z}(t)) = \{\bar{\boldsymbol{w}}_0, ..., \bar{\boldsymbol{w}}_{M-1}\} : [t, t+T_p] \to \mathbb{U}$ with initial condition $\boldsymbol{z}(t)$. The optimal control $\bar{\boldsymbol{w}}^*(\cdot; \boldsymbol{z}(t))$ is the control inputs that minimize the cost function $J(\boldsymbol{z}(t), \bar{\boldsymbol{w}}(\cdot))$ in (60). This was solved by use of the MATLAB function `fmincon` with SQP. The optimal control $\bar{\boldsymbol{w}}^*(\cdot)$ is recalculated over a moving finite horizon T_p, at every sampling instance τ. Its worth noting that the reference $\bar{\boldsymbol{z}}_r$ is constant until next sample $t + \tau$, as seen in (61).

V. Implementation Issues

It will not be possible to command the acceleration of the suspension point directly in a crane control system. Instead, it can be expected that the velocity can be used as an input to the system. This will be the case if the crane has electrical actuators with a velocity loop [18], and it will still be valid if the crane has hydraulic actuators [14].

We therefore propose to integrate the acceleration command to get a velocity command that can be input to a velocity loop in the crane controller. In the simulations this was done by integrating the two acceleration commands $u_x + g_x$ and $u_y + g_y$ to the velocity commands w_x and w_y, and then using w_x and w_y as inputs to the velocity loops, which are modelled as velocity loops for electrical actuators as in [18]. The model that was used is given by

$$\dot{w}_x = u_x + g_x, \quad \dot{w}_y = u_y + g_y \tag{64}$$

$$\ddot{x}_0 = \frac{1}{T_v}(w_x - \dot{x}_0) \tag{65}$$

$$\ddot{y}_0 = \frac{1}{T_v}(w_y - \dot{y}_0) \tag{66}$$

Then if the bandwidth $1/T_v$ of the velocity loop is faster than the bandwidth of the damping controller, the resulting velocities $\dot{x}_0$ and $\dot{y}_0$ will be close to the velocity commands w_x and w_y, and it follows that the accelerations $\ddot{x}_0$ and $\ddot{y}_0$ will be sufficiently close to the commanded accelerations $u_x + g_x$ and $u_y + g_y$.

Another issue is the cancellation terms in the damping controller (15, 16). These terms are small, and due to the exponential stability, it can be expected that these terms can be omitted in practical implementations.

VI. Simulation

A simulation study is done where the commanded path Λ of the suspension point is close to a circle segment resulting from a rotation about the vertical axis of the crane base, where the radius of the circle is $\rho = 20$ m. The reference input $\boldsymbol{z}_r$ is a piece-wise linear approximation of the circular arc. The path Λ and the reference input $\boldsymbol{z}_r$ are shown in Fig. 5 and 6. The trajectory moves from an initial point (20 m, 0) at time $t_{st} = 20$ s to a final point (0, 20 m) at a time $t_{ft} = 55$ s. The trajectory has a maximum velocity $|\bar{v}| = 3.5\gamma$ and max acceleration $|\bar{a}| = \gamma$. The trajectory is based on linear interpolation with parabolic blends for a path with via-points [21].

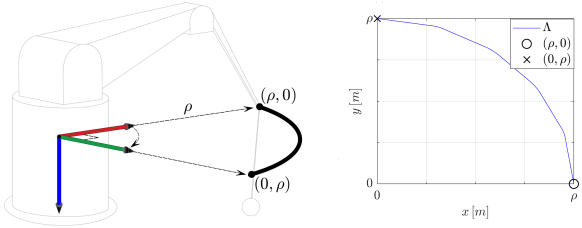

Fig. 5: The path Λ of the reference (x_r, y_r) for the suspension point (x_0, y_0)

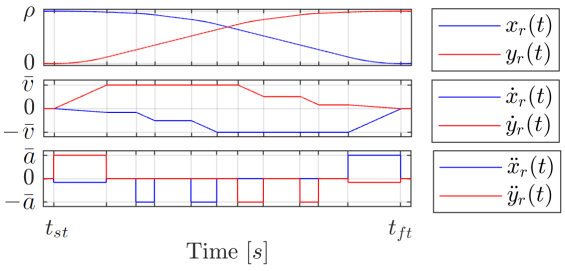

Fig. 6: The reference input $\boldsymbol{z}_r$ with position (x_r, y_r), velocity $(\dot{x}_r, \dot{y}_r)$ and acceleration $(\ddot{x}_r, \ddot{y}_r)$ profiles.

Two different initial condition scenarios were considered in the simulations. In the first scenario the pendulum rotations were initiated at the origin $(\phi_x, \phi_y) = (0, 0)$ and $(\dot{\phi}_x, \dot{\phi}_y) = (0, 0)$. In the second scenario the initial conditions of the pendulum rotations were $(\phi_x, \phi_y) = (15°, -15°)$ and $(\dot{\phi}_x, \dot{\phi}_y) = (0, 0)$. The simulations demonstrated that the controllers gave the desired bounding of the pendulum rotations and a successful tracking of the a desired suspension point trajectory.

The simulations of the model (56) were performed with length of payload $L = 7$ m, time step $h = 0.1$ s, elements $Q_{x_0} = Q_{y_0} = Q_{\dot{x}_0} = Q_{\dot{y}_0} = 1$ of the weighting matrix $\boldsymbol{Q}$, bandwidth $1/T_v = 200$ s^{-1}, perturbations (g_x, g_y) bounded by $\gamma = 0.25$ ms^{-2} and the gains for the control variables (u_x, u_y) were $k_p = 2$ and $k_d = 1$. To achieve a fast controller with ability to continuously sample a new desired reference input $\boldsymbol{z}_r$, the prediction and sampling time were chosen as $T_p = 0.5$ s and $\tau = 0.3$ s.

A. Simulation with zero initial pendulum rotations

A simulation study was done with with zero initial pendulum rotations $(\phi_x, \phi_y) = (0, 0)$. The velocity $(\dot{x}_0, \dot{y}_0)$ in (65, 66), is illustrated in Fig. 7. The velocity was zero until the start time t_{st} of the moving trajectory before it converged to zero after a time t_2.

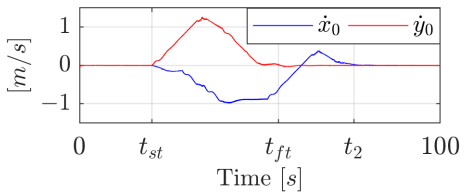

Fig. 7: The velocity $(\dot{x}_0, \dot{y}_0)$ in (65,66) generated from the simulation study in chapter VI-A.

The actual (x_0, y_0) and desired (x_r, y_r) trajectory of the suspension point are illustrated in Fig. 8. The x_0 coordinate deviated slightly from its reference in the time interval $t_{ft} < t < t_2$, while the y_0 coordinate deviated slightly in a time period after t_{st}. The reason for the deviations was the perturbation's (g_x, g_y) input constraint in (58) which limited the nonlinear MPC controller's ability to follow rapid changes in desired position (x_y, y_r) in these time intervals.

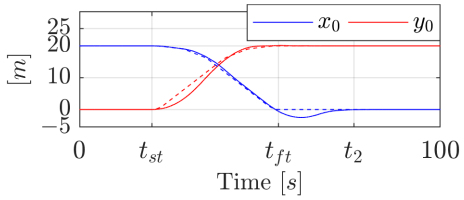

Fig. 8: The actual and desired suspension point trajectory from the simulation study in chapter VI-A. The actual suspension point (x_0, y_0) is represented as solid lines while the desired trajectory (x_r, y_r) is represented as dashed lines.

The pendulum rotations (ϕ_x, ϕ_y) are illustrated in Fig. 9. The pendulum rotations were zero until the start time t_{st} of the commanded motion, and it converged to zero after a time t_2. In the time interval $t_{st} < t < t_2$, the pendulum angles were oscillating because the suspension point was following a moving trajectory in this interval. However, the pendulum rotations were oscillating within $\pm 1°$ since the perturbations (g_x, g_y) were bounded by γ. Its worth noting that the pendulum rotations (ϕ_x, ϕ_y) were oscillating more when the suspension point was deviating more from its reference, due to a more active perturbation (g_x, g_y). At the time t_2, the suspension point reached the static desired position, and the pendulum rotations converged to zero.

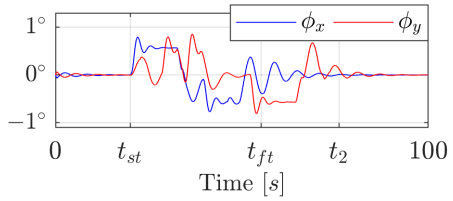

Fig. 9: The resulting pendulum rotations (ϕ_x, ϕ_y) from the simulation study in chapter VI-A

B. Simulation with non-zero initial pendulum rotations

A simulation study was done with initial pendulum rotations $(\phi_x, \phi_y) = (15°, -15°)$. The velocity $(\dot{x}_0, \dot{y}_0)$ in (65, 66), is illustrated in Fig. 10. Compared to the velocity in Section VI-A, the velocity in this case was oscillating in the interval $0 < t < t_{st}$ due to initial pendulum rotations. In the time interval $t > t_{st}$ the velocities in both studies were approximately the same.

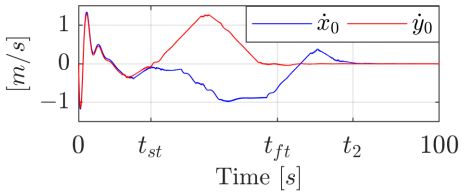

Fig. 10: The velocity $(\dot{x}_0, \dot{y}_0)$ in (65,66) generated from the simulation study in chapter VI-B.

The actual (x_0, y_0) and desired (x_r, y_r) trajectory of the suspension point are illustrated in Fig. 11. Compared to the trajectory (x_0, y_0) in Section VI-A, the trajectory in this case was deviating from the reference in the interval $0 < t < t_{st}$ due to initial pendulum rotations which caused the control variables (u_x, u_y) to be more dominating than the perturbations (g_x, g_y). In the time interval $t > t_{st}$ the trajectories in both studies were approximately the same.

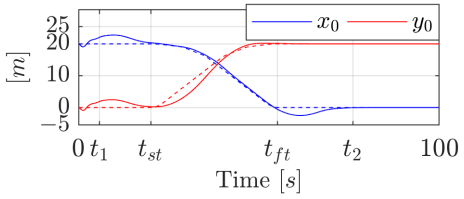

Fig. 11: The actual and desired suspension point trajectory from the simulation study in chapter VI-B. The actual suspension point (x_0, y_0) is represented as solid lines while the desired trajectory (x_r, y_r) is represented as dashed lines.

The pendulum rotations (ϕ_x, ϕ_y) are illustrated in Fig. 12. The pendulum rotations were oscillating within $\pm 1°$ after a time t_1. In the time interval $t > t_{st}$ the pendulum rotations

in both studies were approximately the same, and converged to zero after a time t_2.

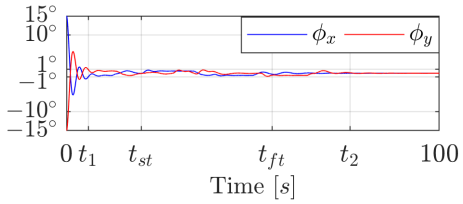

Fig. 12: The resulting pendulum rotations (ϕ_x, ϕ_y) from the simulation study in chapter VI-B

VII. Conclusions

A controller has been developed for the control of the crane load position using a Lyapunov-based pendulum damping controller in an inner loop and a nonlinear MPC position controller in an outer loop. The Lyapunov-based controller was designed to be exponentially stable, so that the state would be ultimately bounded in the presence of a bounded perturbations. Then the position of the crane tip was controlled in an outer loop using a nonlinear MPC where the control variables were the perturbations to the damping controller, which made it possible to limit the perturbations using constraints in the MPC. The performance of the controller was demonstrated in simulations, where the crane tip was moved with a slewing motion of 90° with radius 20 m that was executed in 35 s. The pendulum motions were bounded within $\pm 1°$ while the crane tip was following the trajectory. The pendulum motions converged to zero when the crane tip reached final desired reference.

ACKNOWLEDGMENT

The research presented in this paper was funded by the Norwegian Research Council, SFI Offshore Mechatronics, Project Number 237896.

References

[1] E. M. Abdel-Rahman, A. H. Nayfeh, and Z. N. Masoud. Dynamics and control of cranes: A review. *Modal Analysis*, 9(7):863–908, 2003.

[2] E. Arnold, O. Sawodny, J. Neupert, and K. Schneider. Anti-sway system for boom cranes based on a model predictive control approach. In *IEEE International Conference on Mechatronics and Automation, 2005*, volume 3, pages 1533–1538 Vol. 3, July 2005.

[3] D. Blackburn, J. Lawrence, J. Danielson, W. Singhose, T. Kamoi, and A. Taura. Radial-motion assisted command shapers for nonlinear tower crane rotational slewing. *Control Engineering Practice*, 18(5):523–531, 2010.

[4] C. C. Chung and J. Hauser. Nonlinear control of a swinging pendulum. *Automatica*, 31:851–862, 06 1995.

[5] D. Chwa. Nonlinear tracking control of 3-d overhead cranes against the initial swing angle and the variation of payload weight. *IEEE Transactions on Control Systems Technology*, 17(4):876–883, July 2009.

[6] A. Cibicik, T. A. Myhre, and O. Egeland. Modeling and control of a bifilar crane payload. In *2018 Annual American Control Conference (ACC)*, pages 1305–1312. IEEE, 2018.

[7] Y. Fang, E. Zergeroglu, W. E. Dixon, and D. M. Dawson. Nonlinear coupling control laws for an overhead crane system. In *Proceedings of the 2001 IEEE International Conference on Control Applications (CCA'01) (Cat. No.01CH37204)*, pages 639–644, Sept 2001.

[8] R. Findeisen and F. Allgöwer. An introduction to nonlinear model predictive control. In *21st Benelux Meeting on Systems and Control, Veidhoven*, pages 1–23, 2002.

[9] G. H. Golub and C. F. Van Loan. *Matrix Computations (3rd Ed.)*. Johns Hopkins University Press, Baltimore, MD, USA, 1996.

[10] L. Grüne and J. Pannek. *Nonlinear Model Predictive Control: Theory and Algorithms*. Springer Publishing Company, Incorporated, 2013.

[11] H. Khalil. *Nonlinear Systems*. Pearson Education. Prentice Hall, 2002.

[12] B. Kimiaghalam, A. Homaifar, and B. Sayarrodsari. An application of model predictive control for a shipboard crane. In *Proceedings of the 2001 American Control Conference. (Cat. No.01CH37148)*, volume 2, pages 929–934 vol.2, June 2001.

[13] K. L. Knierim, K. Krieger, and O. Sawodny. Flatness based control of a 3-dof overhead crane with velocity controlled drives. In *IFAC Proceedings*, number 18, pages 363–368. IFAC, 2010.

[14] H. E. Merritt. *Hydraulic control systems*. Wiley, 1967.

[15] A. Mills, A. Wills, and B. Ninness. Nonlinear model predictive control of an inverted pendulum. In *2009 American Control Conference*, pages 2335–2340, June 2009.

[16] J. Neupert, E. Arnold, K. Schneider, and O. Sawodny. Tracking and anti-sway control for boom cranes. *Control Engineering Practice*, 18(1):31–44, 2010.

[17] L. Ramli, Z. Mohamed, A. M. Abdullahi, H. Jaafar, and I. M. Lazim. Review. *Mechanical Systems and Signal Processing*, 95(C):1–23, 2017.

[18] F. Rauscher, S. Nann, and O. Sawodny. Motion control of an overhead crane using a wireless hook mounted IMU. In *2018 Annual American Control Conference (ACC)*, pages 5677–5682. IEEE, 2018.

[19] Y. Sakawa and A. Nakazumi. Modeling and control of a rotary crane. *Journal of Dynamic Systems Measurement and Control*, 107(3):200–206, 1985.

[20] U. Schaper, O. Sawodny, M. Zeitz, and K. Schneider. Load position estimation for crane anti-sway control systems. *Journal of Dynamic Systems Measurement and Control*, 136:031013–1–7, May 2014.

[21] B. Siciliano, L. Sciavicco, L. Villani, and G. Oriolo. *Robotics: Modelling, Planning and Control*. Springer Publishing Company, Incorporated, 1st edition, 2008.

[22] J. Smoczek and J. Szpytko. Particle swarm optimization-based multivariable generalized predictive control for an overhead crane. *IEEE/ASME Transactions on Mechatronics*, 22(1):258–268, Feb 2017.

[23] N. Sun, Y. Fang, and X. Zhang. Energy coupling output feedback control of 4-dof underactuated cranes with saturated inputs. *Automatica*, 49(5):1318–1325, May 2013.

[24] M. Vukov, W. V. Loock, B. Houska, H. Ferreau, J. Swevers, and M. Diehl. Experimental validation of nonlinear mpc on an overhead crane using automatic code generation. In *In Proceedings of the 2012 American Control Conference, Montreal, Canada*, page 62646269, 2012.

[25] J. T. Wen and D. Bayard. A new class of control laws for robotic manipulators - Part I: Non-adaptive case. *International Journal of Control*, 47(5):1361–1385, 1988.

[26] X. Wu and X. He. Partial feedback linearization control for 3-d underactuated overhead crane systems. *ISA transactions*, 65:361370, November 2016.

[27] X. Wu, X. He, N. Sun, and Y. Fang. A novel anti-swing control method for 3-d overhead cranes. In *2014 American Control Conference*, pages 2821–2826, June 2014.

[28] Z. Wu, X. Xia, and B. Zhu. Model predictive control for improving operational efficiency of overhead cranes. *Nonlinear Dynamics*, 79(4):2639–2657, 2015.

[29] K. Yoshida. Nonlinear controller design for a crane system with state constraints. In *Proceedings of the 1998 American Control Conference. ACC (IEEE Cat. No.98CH36207)*, volume 2, pages 1277–1283 vol.2, June 1998.

[30] J. Yu, F. L. Lewis, and T. Huang. Nonlinear feedback control of a gantry crane. In *Proceedings of 1995 American Control Conference - ACC'95*, volume 6, pages 4310–4315 vol.6, June 1995.